Pressure transient analysis of unsteady-state inter-porosity flows for slanted wells in fractured-vuggy carbonate reservoirs

Ren-Shi Nie [a,*], Zipeng Xia [a], Ming Wang [b], Jingcheng Liu [c,d], Tao Zhang [e], Cong Lu [a], Fan-Hui Zeng [a]

a. National Key Laboratory of Oil & Gas Reservoir Geology and Exploitation, Southwest Petroleum University, Chengdu 610500, China
b. Tarim Oilfield Company, PetroChina, Korla, Xinjiang 841000, China
c. Liquor Making Microbial Application & Detection Technology of Luzhou Key Laboratory, Luzhou Vocational & Technical College, Luzhou, 646000, China
d. Institute of Petroleum & Gas Engineering, Chongqing University of Science and Technology, Chongqing, 401331, China
e. Xi'an Sanwei Technology Development Co., LTD, Xi'an, 710021, China

* Corresponding author: [nierenshi2000@126.com] (Ren-Shi Nie)

Keywords

Fractured-vuggy reservoir;
Slanted well;
Triple-porosity model;
Pressure transient analysis;
Interporosity flow;

Abstract

To address the significant challenges posed by multiscale heterogeneity in fractured-vuggy carbonate reservoirs, we have developed a comprehensive triple-porosity pressure transient model specifically tailored for slanted wells. A central innovation of this work is the rigorous incorporation of a unified unsteady-state interporosity flow mechanism. This approach accurately describes the dynamic fluid transfer from both spherical matrix blocks and a distinct vug system into the interconnected natural fracture network, thereby avoiding the limitations of simplified pseudo-steady state assumptions. The model also integrates essential near-wellbore effects such as wellbore storage and skin factor. Leveraging source function theory and the principle of superposition, a new semi-analytical solution was derived in the Laplace domain, with the real-time pressure response obtained via the Stehfest numerical inversion algorithm. Based on this solution, characteristic type curves were generated, revealing a key diagnostic feature: two successive troughs on the pressure derivative plot. These troughs represent the sequential fluid supply, first from the more permeable vugs and subsequently from the low-permeability matrix. Extensive sensitivity analyses systematically quantified the influence of well geometry and critical reservoir parameters on pressure behavior. Finally, a field example from a carbonate reservoir validated the model's practical applicability, demonstrating excellent agreement with actual test data. Consequently, this work offers a more robust tool for well test interpretation in these highly complex formations.

1. Introduction

Naturally fractured-vuggy carbonate reservoirs are a significant source of global hydrocarbon reserves. However, their complex pore structure, characterized by a combination of matrix, fractures, and vugs, presents considerable challenges for accurate reservoir characterization and performance prediction. The dual-porosity model, first proposed by Warren and Root [1], provided a foundational framework for understanding these systems by idealizing them into a high-permeability fracture network and a low-permeability matrix system that acts as a fluid source. This concept has since been extended to more complex representations, such as dual-porosity/dual-permeability models [2,3] and triple-porosity models, which explicitly account for the distinct properties of vugs in addition to fractures and matrix [4]. Recent studies have further elaborated on these complex systems; for instance, Shi et al. [5] established an analytical model for multibranched fault-karst carbonate reservoirs, emphasizing the significant influence of the spatial structure of fracture-cave systems on pressure transient responses.

Concurrently, advances in drilling technology have made slanted, or highly deviated, wells a common strategy for enhancing productivity, especially in thin or dipping formations and for intersecting a greater number of natural fractures. The analysis of pressure transient data from such wells requires specialized models that account for their unique geometry. Early work by Cinco et al. [6] demonstrated that the inclination of a well creates a negative pseudoskin effect. Subsequent research has provided a robust theoretical foundation for slanted well analysis, with Ozkan and Raghavan [7] developing a comprehensive library of source functions in the Laplace domain. This semi-analytical approach remains a powerful tool for solving complex boundary value problems. Recently, Guo et al. [8] applied point-source solutions and the superposition principle to investigate pressure behaviors in heterogeneous multilayered reservoirs. These foundational models have been further adapted to various complex scenarios, including reservoirs with impermeable faults [9] and laminated pay zones [10].

Despite significant progress in modeling both fractured-vuggy reservoirs and slanted wells independently, the intersection of these two areas remains a frontier of active research. Accurately capturing the pressure transient behavior of a slanted well in a triple-porosity system is particularly challenging. While some studies have addressed highly deviated wells in such reservoirs [11–14], they often rely on simplified assumptions for interporosity flow, such as the pseudo-steady state assumption, which may not adequately represent the dynamic fluid exchange between different media during transient tests.

To address this gap, this study develops a comprehensive pressure transient model for a slanted well in a fractured-vuggy carbonate reservoir. The model conceptualizes the formation as a triple-porosity system and, most importantly, incorporates a unified unsteady-state interporosity flow mechanism from both spherical matrix blocks and vugs into the fractures. A semi-analytical solution is derived in the Laplace domain using source function theory, with the corresponding real-time solution obtained via the Stehfest numerical inversion algorithm. Based on the solution, dimensionless type curves of pressure and pressure derivative are generated to identify characteristic flow regimes. Sensitivity analyses are performed to quantify the impact of key reservoir and well parameters. Finally, the proposed model is validated using a field example from a carbonate oil

Accepted by Scientia Iranica

reservoir, confirming its reliability and practical applicability. The established model provides a more robust theoretical basis for well test interpretation and accurate characterization of complex fractured-vuggy carbonate reservoirs.

2. Physical model

(1) A slanted well with a length L, inclination angle θ, and radius r_w is located in a carbonate reservoir with uniform thickness h. The vertical distance from the well center to the reservoir bottom is z_w. (see

Figure 1. Schematic Diagram of the Physical Model for a Slanted Well in a Fractured-Vuggy Carbonate Reservoir

Figure 2. Schematic of Flow Pathways in a Triple-Porosity Single-Permeability Model for a Slanted Well

Figure 3. Schematic of a Matrix Block Model

Figure 4. Flow regime identification on a typical type curve for a slanted well in a triple-porosity reservoir (Roman numerals I–VIII correspond to Stage I–VIII in the text. Other parameters are h = 30m, C_D = 500, θ = 40°, S = 2, λ_{vf} = 10−8, λ_{mf} = 10^{-10}, k_h/k_p = 3, ω_f = 0.01, ω_m = 0.94, ω_v = 0.05, z_{wD} = 0.5, and r_{eD} = 2 × 10^{-4}.).

Figure 5. Pressure transient analysis curves affected by inclination angle of slanted well.(Other parameters are h = 30 m, C_D = 500, S = 2, λ_{vf} = 10^{-8}, λ_{mf} = 10^{-10}, k_h/k_p = 3, ω_f = 0.01, ω_m = 0.94, ω_v = 0.05, z_{wD} = 0.5, and r_{wD} = 2 × 10^{-4}.)

Figure 6. Pressure transient analysis curves affected by length of slanted well.(Other parameters are h = 30 m, C_D = 500, S = 2, θ = 40°, λ_{vf} = 10^{-8}, λ_{mf} = 10^{-10}, k_h/k_p = 3, ω_f = 0.01, ω_m = 0.94, ω_v = 0.05, z_{wD} = 0.5, and r_{wD} = 2 × 10^{-4}.)

Figure 7. Pressure transient analysis curves affected by the vug-fracture interporosity flow coefficient (λ_{vf}).(Other parameters are h = 30 m, C_D = 500, S = 2, θ = 40°, λ_{mf} = 10^{-10}, k_h/k_p = 3, ω_f = 0.01, ω_m = 0.94, ω_v = 0.05, z_{wD} = 0.5, and r_{wD} = 2 × 10^{-4}.)

Figure 8. Pressure transient analysis curves affected by the matrix-fracture interporosity flow coefficient (λ_{mf}).(Other parameters are h = 30 m, C_D = 500, S = 2, θ = 40°, λ_{vf} = 10^{-8}, k_h/k_p = 3, ω_f = 0.01, ω_m = 0.94, ω_v = 0.05, z_{wD} = 0.5, and r_{wD} = 2×10^{-4}.)

Figure 9. Pressure transient analysis curves affected by the vuggy storativity ratio (ω_v).(Other parameters are h = 30 m, C_D = 500, S = 2, θ = 40°, λ_{vf} = 10^{-8}, λ_{mf} = 10^{-10}, k_h/k_p = 5, ω_f = 0.01, z_{wD} = 0.5, and r_{wD} = 2 × 10^{-4}.)

Figure 10. Pressure transient analysis curves affected by the fracture storativity ratio (ω_f).(Other parameters are h = 30 m, C_D = 500, S = 2, θ = 40°, λ_{vf} = 10^{-8}, λ_{mf} = 10^{-10}, k_h/k_p = 5, ω_v = 0.05, z_{wD} = 0.5, and r_{wD} = 2 × 10^{-4}.)

Figure 11. Fitted curves for the established model and the field data

List of Table Captions

Table 1. Formation and well parameters

Table 2. Well-test interpretation parameters

Accepted by Scientia Iranica

)
(2) The carbonate reservoir consists of three porous media systems: matrix, natural fractures, and dissolution vugs. It is assumed that the permeability of natural fractures is greater than that of dissolution vugs, and the permeability of dissolution vugs is greater than that of the matrix micropores. Only the natural fractures are considered to be connected to the slanted well. This assumption is based on the physical reality of fractured-vuggy carbonate reservoirs, where the permeability of the fracture network is typically orders of magnitude higher than that of the matrix or isolated vugs. Consequently, fractures serve as the primary global flow conduits, while matrix blocks and vugs act as local storage sources feeding into the fracture network.The direct fluid supply from the matrix and dissolution vugs to the well is neglected, as is the crossflow between the matrix and the dissolution vugs. The matrix and the vugs act as fluid sources that supply the natural fractures. Fluid first flows from the dissolution vugs to the fractures, followed by flow from the matrix, and then enters the slanted wellbore through the fractures. (see **Figure 2**)
(3) A unified transient interporosity flow mechanism is adopted for the model. This approach treats the fractured-vuggy formation as a composite of three overlapping, continuous media (a triple-porosity/single-permeability system). The spatial relationship is conceptualized within a representative elementary volume (REV), where spherical matrix blocks and vugs are considered to be uniformly distributed throughout the fracture network. Both the matrix blocks and the dissolution vugs are assumed to be spherical in shape (see **Figure 3**), with their respective shape factors denoted by αm and αv. Consequently, the flow from both the matrix and vuggy systems into the natural fracture network is considered to be transient (unsteady-state). This assumption implies that a pressure drop develops within each element, and the internal pressure is therefore a function of both time and spatial location, exhibiting a spherically symmetric distribution with respect to the element's center.
(4) The top and bottom of the carbonate reservoir are considered impermeable. In the horizontal direction, three types of outer boundary conditions are considered: infinite boundary, constant pressure boundary, and closed boundary.
(5) The slanted well produces at a constant rate q, and both wellbore storage effect and skin effect are taken into account.
(6) Reservoir and fluid properties, including oil viscosity (μ), wellbore storage coefficient (C_s), total compressibility (C_t), skin factor (S), horizontal permeability (k_h), and perpendicular permeability (k_p), are all assumed to be constant.

3. Mathematical Models

3.1. Mathematical model for triple-porosity reservoir

The model considers a system of spherical matrix blocks and dissolution vugs with radii of r_{ms} and r_{vs}, respectively, within which the pressure distribution is assumed to be spherically symmetric. Single-phase crude oil, originating from the centers of these elements, undergoes transient interporosity flow into the natural fracture network and subsequently flows through the fractures to the wellbore. At the matrix-fracture and vug-fracture interfaces, a pressure continuity condition is imposed: the pressure at the surface of the matrix blocks (p_m) and the vugs (p_v) is assumed to be equal to the pressure in the natural fractures (p_f). Let q_m and q_v denote the volumetric source terms, defined as the volume of fluid flowing from the matrix blocks and vugs, respectively, per unit time and per unit bulk volume.

In this model, both matrix blocks and dissolution vugs are idealized as spheres to facilitate the derivation of the analytical solution. It is acknowledged that in realistic fractured-vuggy reservoirs, these porous media may exhibit diverse geometries, such as slabs (fracture-bounded sheets) or sticks (fracture-bounded columns). The choice of geometry primarily affects the interporosity flow shape factor (α) and the specific form of the transfer function $f(u)$ in the Laplace domain. For example, while spherical blocks yield a specific transfer function involving hyperbolic cotangents, slab or stick geometries would result in different functional forms, leading to variations in the timing and rate of the transient interporosity flow. However, despite these quantitative differences, the fundamental qualitative behavior—specifically the presence of distinct flow regimes and the characteristic "double-trough" signature on the pressure derivative curve—is expected to remain consistent across different geometries, representing the sequential fluid transfer inherent to triple-porosity systems.

According to Darcy's Law, the seepage velocity at the surface of the spherical matrix block (where $r_m = r_{ms}$) is given by:

$$v_m = -\frac{k_m}{\mu}\left(\frac{\partial p_m}{\partial r_m}\right)\Big|_{r_m = r_{ms}} \tag{1}$$

According to Darcy's Law, the seepage velocity at the surface of the spherical dissolution vug (where $r_v = r_{vs}$) is given by:

$$v_v = -\frac{k_v}{\mu}\left(\frac{\partial p_v}{\partial r_v}\right)\Big|_{r_v = r_{vs}} \tag{2}$$

The seepage velocity at the surface of a spherical matrix block or dissolution vug is equal to the volumetric flow rate from the element divided by its surface area. That is, for a spherical matrix block:

$$v_m = \left(\frac{4}{3}\pi r_{ms}^{\ 3} q_m\right)\Big/\left(4\pi r_{ms}^{\ 2}\right) = \frac{1}{3} r_{ms} q_{ms} \tag{3}$$

$$v_v = \left(\frac{4}{3}\pi r_{vs}^{\ 3} q_v\right)\Big/\left(4\pi r_{vs}^{\ 2}\right) = \frac{1}{3} r_{vs} q_{vs} \tag{4}$$

Combining **Eq.(3)** with **Eq.(4)** yields the coupling condition that governs the interporosity flow from the matrix blocks and dissolution vugs into the natural fracture network:

Accepted by Scientia Iranica

$$q_{\mathrm{m}} = -\frac{3}{r_{\mathrm{ms}}}\frac{k_{\mathrm{m}}}{\mu}\left(\frac{\partial p_{\mathrm{m}}}{\partial r_{\mathrm{m}}}\right)\Big|_{r_{\mathrm{m}}=r_{\mathrm{ms}}} \tag{5}$$

$$q_{v} = -\frac{3}{r_{\mathrm{vs}}}\frac{k_{v}}{\mu}\left(\frac{\partial p_{v}}{\partial r_{v}}\right)\Big|_{r_{v}=r_{\mathrm{vs}}} \tag{6}$$

Flow Model for the Matrix System

The governing flow equation for the matrix system is:

$$\frac{\partial^2 p_{\mathrm{m}}}{\partial {r_{\mathrm{m}}}^2} + \frac{2}{r_{\mathrm{m}}}\frac{\partial p_{\mathrm{m}}}{\partial r_{\mathrm{m}}} = \frac{\mu\phi_{\mathrm{m}}C_{\mathrm{mt}}}{3.6k_{\mathrm{m}}}\frac{\partial p_{\mathrm{m}}}{\partial t} \qquad (0 < r_{\mathrm{m}} < r_2) \tag{7}$$

The initial condition for the matrix system is:

$$p_{\mathrm{m}}\big|_{t=0} = p_{\mathrm{i}} \tag{8}$$

The inner boundary condition at the center of the spherical matrix block is:

$$\frac{\partial p_{\mathrm{m}}}{\partial r_{\mathrm{m}}}\Big|_{r_{\mathrm{m}}=0} = 0 \tag{9}$$

The outer boundary coupling condition at the surface of the spherical matrix block is:

$$p_{\mathrm{m}}(r_{\mathrm{m}}, t)\Big|_{r_{\mathrm{m}}=r_2} = p_{\mathrm{f}} \tag{10}$$

Flow Model for the Vuggy System

The governing flow equation for the vuggy system is:

$$\frac{\partial^2 p_{v}}{\partial {r_{v}}^2} + \frac{2}{r_{v}}\frac{\partial p_{v}}{\partial r_{v}} = \frac{\mu\phi_{v}C_{\mathrm{vt}}}{3.6k_{v}}\frac{\partial p_{v}}{\partial t} \qquad (0 < r_{v} < r_2) \tag{11}$$

The initial condition for the vuggy system is:

$$p_{v}\big|_{t=0} = p_{\mathrm{i}} \tag{12}$$

The inner boundary condition at the center of the spherical dissolution vug is:

$$\frac{\partial p_{v}}{\partial r_{v}}\Big|_{r_{v}=0} = 0 \tag{13}$$

The outer boundary coupling condition at the surface of the spherical dissolution vug is:

$$p_{v}(r_{v}, t)\Big|_{r_{v}=r_2} = p_{\mathrm{f}} \tag{14}$$

Flow Model for the Natural Fracture System

The governing partial differential equation for the natural fracture system is:

$$\left(\frac{\partial^2 p_{\mathrm{f}}}{\partial r^2} + \frac{1}{r}\frac{\partial p_{\mathrm{f}}}{\partial r} + \frac{k_{\mathrm{fp}}}{k_{\mathrm{fh}}}\frac{\partial^2 p_{\mathrm{f}}}{\partial z^2}\right) + \frac{\mu}{k_{\mathrm{fh}}}(q_{\mathrm{m}} + q_{\mathrm{v}}) = \frac{\mu\phi_{\mathrm{f}}C_{\mathrm{ft}}}{3.6k_{\mathrm{fh}}}\frac{\partial p_{\mathrm{f}}}{\partial t} \tag{15}$$

The initial condition for the natural fracture system is:

$$p_{\mathrm{f}}\big|_{t=0} = p_{\mathrm{i}} \tag{16}$$

The inner boundary condition for a point source with a constant production rate is:

$$\tilde{q} = \lim_{\varepsilon\to 0}\left(\lim_{r\to 0}\frac{k_{\mathrm{fh}}}{1.842\times 10^{-3}\mu\varepsilon}\int_{z_{\mathrm{w}}-\varepsilon/2}^{z_{\mathrm{w}}+\varepsilon/2} r\frac{\partial p_{\mathrm{f}}}{\partial r}\mathrm{d}z\right) \tag{17}$$

The outer boundary conditions are:

Top Boundary (No-Flow):

$$\frac{\partial p_{\mathrm{f}}}{\partial z}\Big|_{z=h} = 0 \tag{18}$$

Bottom Boundary (No-Flow):

$$\frac{\partial p_{\mathrm{f}}}{\partial z}\Big|_{z=0} = 0 \tag{19}$$

Lateral Boundary Condition:

$$\lim_{r\to\infty} p_{\mathrm{f}}(r, z, t) = p_{\mathrm{i}} \ \text{(infinite)} \tag{20}$$

$$p_{\mathrm{f}}\Big|_{r=r_{\mathrm{e}}} = p_{\mathrm{i}} \ \text{(constant pressure)} \tag{21}$$

Accepted by Scientia Iranica

$$\frac{\partial p_{\mathrm{f}}}{\partial r}\Big|_{r=r_{\mathrm{e}}}=0\quad\text{(closed)}\tag{22}$$

The total production rate of the slanted well is obtained by integrating the point source flux along the wellbore:

$$q=\int_{-L\sin\theta/2}^{L\sin\theta/2}\frac{1}{\sin\theta}\tilde{q}(r,t)\mathrm{d}x\tag{23}$$

$$p_{\mathrm{w}}\big|_{r\to 0}=\int_{-L\sin\theta/2}^{L\sin\theta/2}\frac{1}{\sin\theta}p_{\mathrm{f}}(r,t)\mathrm{d}x\tag{24}$$

3.2. Dimensionless mathematical model

Dimensionless parameters definition is shown in the **Appendix Parameters definition**. After the dimensionless transformation, the model is listed below:

Flow Model for the Matrix System

The governing flow equation for the matrix system is:

$$\frac{\partial^2 p_{\mathrm{mD}}}{\partial {r_{\mathrm{mD}}}^2}+\frac{2}{r_{\mathrm{mD}}}\frac{\partial p_{\mathrm{mD}}}{\partial r_{\mathrm{mD}}}=\frac{15\omega_{\mathrm{m}}}{\lambda_{\mathrm{m}}}\frac{\partial p_{\mathrm{mD}}}{\partial t_{\mathrm{D}}}\qquad(0<r_{\mathrm{mD}}<1)\tag{25}$$

The initial condition for the matrix system is:

$$p_{\mathrm{mD}}\big|_{t_{\mathrm{D}}=0}=0\tag{26}$$

Inner Boundary Condition:

$$\frac{\partial p_{\mathrm{mD}}}{\partial r_{\mathrm{mD}}}\Big|_{r_{\mathrm{mD}}=0}=0\tag{27}$$

Outer Boundary Coupling Condition:

$$p_{\mathrm{mD}}(r_{\mathrm{mD}},t_{\mathrm{D}})\big|_{r_{\mathrm{mD}}=r_{\mathrm{msD}}}=p_{\mathrm{fD}}\tag{28}$$

Flow Model for the Vuggy System

The governing flow equation for the vuggy system is:

$$\frac{\partial^2 p_{\mathrm{vD}}}{\partial {r_{\mathrm{vD}}}^2}+\frac{2}{r_{\mathrm{vD}}}\frac{\partial p_{\mathrm{vD}}}{\partial r_{\mathrm{vD}}}=\frac{15\omega_{v}}{\lambda_{v}}\frac{\partial p_{\mathrm{vD}}}{\partial t_{\mathrm{D}}}\qquad(0<r_{\mathrm{vD}}<1)\tag{29}$$

The initial condition for the vuggy system is:

$$p_{\mathrm{vD}}\big|_{t_{\mathrm{D}}=0}=0\tag{30}$$

Inner Boundary Condition:

$$\frac{\partial p_{\mathrm{vD}}}{\partial r_{\mathrm{vD}}}\Big|_{r_{\mathrm{vD}}=0}=0\tag{31}$$

Outer Boundary Coupling Condition:

$$p_{\mathrm{vD}}(r_{\mathrm{vD}},t_{\mathrm{D}})\big|_{r_{\mathrm{vD}}=r_{\mathrm{vsD}}}=p_{\mathrm{fD}}\tag{32}$$

Flow Model for the Natural Fracture System

The governing partial differential equation for the natural fracture system is:

$$\frac{\partial^2 p_{\mathrm{fD}}}{\partial {r_{\mathrm{D}}}^2}+\frac{1}{r_{\mathrm{D}}}\frac{\partial p_{\mathrm{fD}}}{\partial r_{\mathrm{D}}}+\frac{1}{h_{\mathrm{D}}^2}\frac{\partial^2 p_{\mathrm{fD}}}{\partial {z_{\mathrm{D}}}^2}-\frac{1}{5}\lambda_{\mathrm{mf}}\frac{\partial p_{\mathrm{mD}}}{\partial r_{\mathrm{mD}}}\Big|_{r_{\mathrm{mD}}=1}-\frac{1}{5}\lambda_{\mathrm{vf}}\frac{\partial p_{\mathrm{vD}}}{\partial r_{\mathrm{vD}}}\Big|_{r_{\mathrm{vD}}=1}=\omega_{\mathrm{f}}\frac{\partial p_{\mathrm{fD}}}{\partial t_{\mathrm{D}}}\tag{33}$$

Model Auxiliary Conditions:

Initial Condition:

$$p_{\mathrm{fD}}\big|_{t_{\mathrm{D}}=0}=0\tag{34}$$

Inner Boundary Condition (Constant-Rate Production):

$$\lim_{r_{\mathrm{D}}\to 0}\left(r_{\mathrm{D}}\frac{\partial p_{\mathrm{fD}}}{\partial r_{\mathrm{D}}}\right)=-1\tag{35}$$

Outer Boundary Conditions:

Top Boundary (No-Flow):

$$\frac{\partial p_{\mathrm{fD}}}{\partial z_{\mathrm{D}}}\Big|_{z_{\mathrm{D}}=1}=0\tag{36}$$

Bottom Boundary (No-Flow):

Accepted by Scientia Iranica

$$\frac{\partial p_{\mathrm{fD}}}{\partial z_{\mathrm{D}}}\Big|_{z_{\mathrm{D}}=0}=0 \tag{37}$$

Lateral Boundary:

$$\lim_{r_{\mathrm{D}}\to\infty} p_{\mathrm{fD}}=0(\text{infinite}) \tag{38}$$

$$p_{\mathrm{fD}}\Big|_{r_{\mathrm{D}}=r_{\mathrm{eD}}}=0 \ \ (\text{constant pressure}) \tag{39}$$

$$\frac{\partial p_{\mathrm{fD}}}{\partial r_{\mathrm{D}}}\Big|_{r_{\mathrm{D}}=r_{\mathrm{eD}}}=0\ (\text{closed}) \tag{40}$$

4. Solving model

4.1. Model transformation

Laplace transform formula is shown below:

$$L[p_{\mathrm{D}}(r_{\mathrm{D}},t_{\mathrm{D}})]=\overline{p}_{\mathrm{D}}(r_{\mathrm{D}},u)=\int_0^{\infty} p_{\mathrm{D}}(r_{\mathrm{D}},t_{\mathrm{D}})\mathrm{e}^{-ut_{\mathrm{D}}}\mathrm{d}t_{\mathrm{D}} \tag{41}$$

Using the above formula, the model becomes:

$$\frac{\partial^2 \overline{p}_{\mathrm{mD}}}{\partial {r_{\mathrm{mD}}}^2}+\frac{2}{r_{\mathrm{mD}}}\frac{\partial \overline{p}_{\mathrm{mD}}}{\partial r_{\mathrm{mD}}}=\frac{15\omega_{\mathrm{m}}u}{\lambda_{\mathrm{m}}}\overline{p}_{\mathrm{mD}} \qquad (0<r_{\mathrm{mD}}<1) \tag{42}$$

$$\frac{\partial \overline{p}_{\mathrm{mD}}}{\partial r_{\mathrm{mD}}}\Big|_{r_{\mathrm{mD}}=0}=0 \tag{43}$$

$$\overline{p}_{\mathrm{mD}}(r_{\mathrm{mD}},t_{\mathrm{D}})\Big|_{r_{\mathrm{mD}}=r_{\mathrm{msD}}}=\overline{p}_{\mathrm{fD}} \tag{44}$$

$$\frac{\partial^2 \overline{p}_{\mathrm{vD}}}{\partial {r_{\mathrm{vD}}}^2}+\frac{2}{r_{\mathrm{vD}}}\frac{\partial \overline{p}_{\mathrm{vD}}}{\partial r_{\mathrm{vD}}}=\frac{15\omega_{\mathrm{v}}u}{\lambda_{\mathrm{v}}}\overline{p}_{\mathrm{vD}} \qquad (0<r_{\mathrm{vD}}<1) \tag{45}$$

$$\frac{\partial \overline{p}_{\mathrm{vD}}}{\partial r_{\mathrm{vD}}}\Big|_{r_{\mathrm{vD}}=0}=0 \tag{46}$$

$$\overline{p}_{\mathrm{vD}}(r_{\mathrm{vD}},t_{\mathrm{D}})\Big|_{r_{\mathrm{vD}}=r_{\mathrm{vsD}}}=\overline{p}_{\mathrm{fD}} \tag{47}$$

$$\frac{\partial^2 \overline{p}_{\mathrm{fD}}}{\partial {r_{\mathrm{D}}}^2}+\frac{1}{r_{\mathrm{D}}}\frac{\partial \overline{p}_{\mathrm{fD}}}{\partial r_{\mathrm{D}}}+\frac{1}{h_{\mathrm{D}}^2}\frac{\partial^2 \overline{p}_{\mathrm{fD}}}{\partial {z_{\mathrm{D}}}^2}-\frac{1}{5}\lambda_{\mathrm{mf}}\frac{\partial p_{\mathrm{mD}}}{\partial r_{\mathrm{mD}}}\Big|_{r_{\mathrm{mD}}=1}-\frac{1}{5}\lambda_{\mathrm{vf}}\frac{\partial p_{\mathrm{vD}}}{\partial r_{\mathrm{vD}}}\Big|_{r_{\mathrm{vD}}=1}=u\omega_{\mathrm{f}}\overline{p}_{\mathrm{fD}} \tag{48}$$

$$\lim_{r_{\mathrm{D}}\to 0}(r_{\mathrm{D}}\frac{\partial \overline{p}_{\mathrm{fD}}}{\partial r_{\mathrm{D}}})=-\frac{1}{u} \tag{49}$$

$$\frac{\partial \overline{p}_{\mathrm{fD}}}{\partial z_{\mathrm{D}}}\Big|_{z_{\mathrm{D}}=1}=0 \tag{50}$$

$$\frac{\partial \overline{p}_{\mathrm{fD}}}{\partial z_{\mathrm{D}}}\Big|_{z_{\mathrm{D}}=0}=0 \tag{51}$$

$$\lim_{r_{\mathrm{D}}\to\infty} \overline{p}_{\mathrm{fD}}=0 \ \ (\text{infinite}) \tag{52}$$

$$\overline{p}_{\mathrm{fD}}\Big|_{r_{\mathrm{D}}=r_{\mathrm{eD}}}=0 \ \ (\text{constant pressure}) \tag{53}$$

$$\frac{\partial \overline{p}_{\mathrm{fD}}}{\partial r_{\mathrm{D}}}\Big|_{r_{\mathrm{D}}=r_{\mathrm{eD}}}=0\ (\text{closed}) \tag{54}$$

4.2. Solution to this model

By substituting the solutions of **Eq.(42)** and (**45**)into **Eq.(48)**, we obtain:

$$\frac{\partial^2 \overline{p}_{\mathrm{fD}}}{\partial {r_{\mathrm{D}}}^2}+\frac{1}{r_{\mathrm{D}}}\frac{\partial \overline{p}_{\mathrm{fD}}}{\partial r_{\mathrm{D}}}+\frac{1}{h_{\mathrm{D}}^2}\frac{\partial^2 \overline{p}_{\mathrm{fD}}}{\partial {z_{\mathrm{D}}}^2}-f(u)\overline{p}_{\mathrm{fD}}=0 \tag{55}$$

The separation of variable formula is shown below:

Accepted by Scientia Iranica

$$\overline{p}_{\mathrm{fD}} = \overline{R}(r_{\mathrm{D}})\overline{Z}(z_{\mathrm{D}}) \tag{56}$$

Substitute **Eq.(55)** into **Eq.(56)**:

$$\overline{R}''\overline{Z} + \frac{1}{r_{\mathrm{D}}}\overline{R}'\overline{Z} + \frac{1}{h_{\mathrm{D}}^2}\overline{R}\overline{Z}'' - f(u)\overline{R}\overline{Z} = 0 \tag{57}$$

$$h_{\mathrm{fD}}^2 \frac{\overline{R}'' + \frac{1}{r_{\mathrm{D}}}\overline{R}' - f(u)\overline{R}}{\overline{R}} = -\frac{\overline{Z}''}{\overline{Z}} = \lambda \tag{58}$$

$$f(u) = \frac{1}{5}\lambda_{\mathrm{vf}}[\sigma_{\mathrm{v}}\mathrm{cth}(\sigma_{\mathrm{v}}) - 1] + \frac{1}{5}\lambda_{\mathrm{mf}}[\sigma_{\mathrm{m}}\mathrm{cth}(\sigma_{\mathrm{m}}) - 1] + \omega_{\mathrm{f}} u \tag{59}$$

Then

$$\overline{R}'' + \frac{1}{r_{\mathrm{D}}}\overline{R}' - \xi\overline{R} = 0 \tag{60}$$

$$\xi = f(u) + \frac{\lambda}{h_{\mathrm{D}}^2} \tag{61}$$

$$\overline{Z}'' + \lambda\overline{Z} = 0 \tag{62}$$

(1) The solution in the horizontal direction

The general solution of **Eq.(60)** can be obtained:

$$\overline{R} = A\mathrm{I}_0(r_{\mathrm{D}}\sqrt{\xi}) + B\mathrm{K}_0(r_{\mathrm{D}}\sqrt{\xi}) \tag{63}$$

So the first derivative takes the form:

$$\overline{R}' = A\sqrt{\xi}\mathrm{I}_1(r_{\mathrm{D}}\sqrt{\xi}) - B\sqrt{\xi}\mathrm{K}_1(r_{\mathrm{D}}\sqrt{\xi}) \tag{64}$$

Substitute **Eq.(64)** into **Eq.(49)**:

$$\lim_{r_{\mathrm{D}}\to 0}[r_{\mathrm{D}}\sqrt{\xi}\mathrm{I}_1(r_{\mathrm{D}}\sqrt{\xi})A - r_{\mathrm{D}}\sqrt{\xi}\mathrm{K}_1(r_{\mathrm{D}}\sqrt{\xi})B] = -\frac{1}{u} \tag{65}$$

The properties of the Bessel function are listed below:

$$\lim_{x\to\infty}\mathrm{I}_0(x) \to \infty, \lim_{x\to\infty}\mathrm{K}_0(x) = 0, \lim_{x\to 0}\mathrm{I}_1(x) = 0, \lim_{x\to 0}x\mathrm{K}_1(x) = 1 \tag{66}$$

So according to **Eq.(66)**, the **Eq.(65)** becomes:

$$B = \frac{1}{u} \tag{67}$$

Substitute **Eq.(63)** into the side external boundary conditions **Eqs.(**(52)~(54)**)**:

$$\lim_{r_{\mathrm{D}}\to\infty}[A\mathrm{I}_0(r_{\mathrm{D}}\sqrt{\xi}) + B\mathrm{K}_0(r_{\mathrm{D}}\sqrt{\xi})] = 0 \quad \text{(infinite)} \tag{68}$$

$$A\mathrm{I}_0(r_{\mathrm{eD}}\sqrt{\xi}) + B\mathrm{K}_0(r_{\mathrm{eD}}\sqrt{\xi}) = 0 \quad \text{(constant pressure)} \tag{69}$$

$$A\sqrt{\xi}\mathrm{I}_1(r_{\mathrm{eD}}\sqrt{\xi}) - B\sqrt{\xi}\mathrm{K}_1(r_{\mathrm{eD}}\sqrt{\xi}) = 0 \quad \text{(closed)} \tag{70}$$

So according to **Eq.(66)**:

$$A = 0 \quad \text{(infinite)} \tag{71}$$

$$A = -\frac{1}{u}\frac{\mathrm{K}_0(r_{\mathrm{eD}}\sqrt{\xi})}{\mathrm{I}_0(r_{\mathrm{eD}}\sqrt{\xi})} \quad \text{(constant pressure)} \tag{72}$$

$$A = \frac{1}{u}\frac{\mathrm{K}_1(r_{\mathrm{eD}}\sqrt{\xi})}{\mathrm{I}_1(r_{\mathrm{eD}}\sqrt{\xi})} \quad \text{(closed)} \tag{73}$$

(2) The solution in the perpendicular direction

The general solution of **Eq.(62)** can be obtained:

$$\overline{Z} = C\cos(\sqrt{\lambda}z_{\mathrm{D}}) + D\sin(\sqrt{\lambda}z_{\mathrm{D}}) \tag{74}$$

So the first derivative of **Eq.(74)** can be written as:

$$\overline{Z}' = -\sqrt{\lambda}\left[C\sin(\sqrt{\lambda}z_{\mathrm{D}}) - D\cos(\sqrt{\lambda}z_{\mathrm{D}})\right] \tag{75}$$

Substitute **Eq.(75)** into **Eq.(50)** and **Eq.(51)**:

Accepted by Scientia Iranica

$$\overline{Z}'\Big|_{z_{\mathrm{D}}=0} = -C\sqrt{\lambda}\sin(\sqrt{\lambda}\cdot 0) + D\sqrt{\lambda}\cos(\sqrt{\lambda}\cdot 0) = 0 \tag{76}$$

$$\overline{Z}'\Big|_{z_{\mathrm{D}}=1} = -C\sqrt{\lambda}\sin(\sqrt{\lambda}) + D\sqrt{\lambda}\cos(\sqrt{\lambda}) = 0 \tag{77}$$

Combine **Eq.(76)** and **Eq.(77)**:

$$D=0,\ \lambda = (n\pi)^2, n = 0,1,2\ldots \tag{78}$$

In the above equations, $\cos(\sqrt{\lambda} z_{\mathrm{D}})$ is the eigenfunction and λ is the eigenvalue for closed top and bottom boundaries. In addition, z_{D} is equal to z_{wD} for the wellbore center. Because the slanted well produces at a constant rate, the PDC will be close to the '1/2' line. Then the other coefficient can be determined as:

$$C=\frac{1}{2}\cos(\sqrt{\lambda_n} z_{\mathrm{wD}}), \lambda_n = (n\pi)^2, n = 0,1,2\ldots \tag{79}$$

So the solution in the vertical direction can be written as:

$$\overline{Z} = \frac{1}{2}\cos(n\pi z_{\mathrm{wD}})\cos(n\pi z_{\mathrm{D}}), n = 0,1,2\ldots \tag{80}$$

(3) The bottom-hole pressure solution of slanted well

The pressure solution of fracture can be written as:

$$\overline{p}_{\mathrm{fD}} = \overline{R}\cdot\overline{Z} = \frac{1}{2}\sum_{n=0}^{\infty}[A_n \mathrm{I}_0(r_{\mathrm{D}}\sqrt{\xi_n}) + B_n \mathrm{K}_0(r_{\mathrm{D}}\sqrt{\xi_n})]\cos(n\pi z_{\mathrm{wD}})\cos(n\pi z_{\mathrm{D}}) \tag{81}$$

Where

$$\xi_n = f(u) + \frac{(n\pi)^2}{h_{\mathrm{D}}^2}, A_n = A, B_n = B, n = 0,1,2\ldots \tag{82}$$

At the wellbore

$$r_{\mathrm{D}} = \sqrt{x_{\mathrm{D}}^2 + y_{\mathrm{D}}^2}, y_{\mathrm{D}} = 0, z_{\mathrm{D}} = \frac{r_{\mathrm{w}}}{h} + z_{\mathrm{wD}} \tag{83}$$

By superposition integrals along the slanted well direction, the bottom-hole pressure solution of a slanted well will be acquired:

$$\begin{aligned}\overline{p}_{\mathrm{sD}} = \frac{1}{2}\sum_{n=0}^{\infty}[A_n \int_{-L\sin\theta/2/r_{\mathrm{w}}}^{L\sin\theta/2/r_{\mathrm{w}}} \frac{1}{\sin\theta}\mathrm{I}_0(x_{\mathrm{D}}\sqrt{\xi_n})\mathrm{d}x_{\mathrm{D}} + \\ B_n \int_{-L\sin\theta/2/r_{\mathrm{w}}}^{L\sin\theta/2/r_{\mathrm{w}}} \frac{1}{\sin\theta}\mathrm{K}_0(x_{\mathrm{D}}\sqrt{\xi_n})\mathrm{d}x_{\mathrm{D}}]\cos(n\pi z_{\mathrm{wD}})\cos[n\pi(\frac{r_{\mathrm{w}}}{h} + z_{\mathrm{wD}})]\end{aligned} \tag{84}$$

Due to the existence of WSE(wellbore storage effect), the pressure solution of this model under real conditions can be acquired by the following formula:

$$\overline{p}_{\mathrm{wD}} = \frac{\overline{p}_{\mathrm{sD}}}{1 + C_{\mathrm{D}}u^2\overline{p}_{\mathrm{sD}}} \tag{85}$$

5. Pressure transient characteristics

5.1. Flow Regime Identification

Based on the semi-analytical solution, a typical log-log plot of dimensionless pressure and its derivative reveals a unique sequence of up to eight distinct flow regimes (**Figure 4**). At very early times, the flow is dominated by wellbore storage (Stage I), characterized by a unit-slope line on the derivative curve. This is followed by a transitional period (Stage II) reflecting the influence of the skin factor. As the pressure transient propagates into the formation, it first induces pseudo-radial flow within the high-conductivity fracture network (Stage III), the behavior of which is governed by the properties of the interconnected fractures, including their orientation and conductivity [15,16]. Subsequently, a pressure differential develops between the fractures and the more permeable vugs, initiating the first unsteady-state interporosity flow from vugs to fractures (Stage IV); this process is analogous to the fluid exchange modeled in various dual-porosity systems, from hydrocarbon reservoirs to aquifers [17–20]. Once the fracture-vug system reaches equilibrium, a second, intermediate pseudo-radial flow regime (Stage V) emerges, reflecting their combined hydraulic response of the fracture and vug systems. [21]. With continued pressure depletion, the low-permeability matrix begins to feed fluid into the fractures, creating a second, more pronounced unsteady-state interporosity flow transition (Stage VI), which forms the characteristic second trough. The appearance of these "double troughs" is the key diagnostic feature of a triple-porosity system. At late times, all three media contribute to flow collectively, leading to the total system pseudo-radial flow (Stage VII), reflecting the bulk properties of the composite reservoir system as seen by the slanted or fractured well [22,23]. Finally, the pressure transient may reach the reservoir's outer limits, resulting in boundary-dominated flow (Stage VIII), which can be influenced by reservoir heterogeneity and the specific configuration of the discrete fracture

Accepted by Scientia Iranica

network [24,25]. The precise identification of this sequence, especially the two interporosity flow troughs, is crucial for accurately characterizing the complex dynamics of fractured-vuggy reservoirs.

5.2. Curves sensitivity analysis of triple-medium model

Figure 5 illustrates a sensitivity analysis on the well inclination angle, θ, for a slanted well completed in a triple-porosity, single-permeability reservoir. The results demonstrate a clear trend: as the inclination angle increases, the pressure and pressure derivative curves shift systematically downward. This effect is most evident during the early- to middle-time flow periods, specifically encompassing Flow Regimes I, II, and III.

Figure 6 presents a sensitivity analysis of the slanted well length, L, for a well completed in a triple-porosity, single-permeability reservoir. The results indicate that the well length most profoundly affects the early- to middle-time flow periods, namely Flow Regimes I, II, and III. Specifically, an increase in the slanted well length not only causes a downward shift in both the pressure and pressure derivative curves but also extends the duration of Flow Regime IV.

Figure 7 illustrates the influence of the vug-fracture interporosity flow coefficient, (λvf), on the transient pressure response. As observed, λ_{vf} primarily governs the characteristics of the first interporosity flow transition from the vug system to the fractures. Its influence is negligible during the early-time flow regimes, including wellbore storage (Stage I) and fracture system pseudo-radial flow (Stage III), as these stages are dominated by wellbore and fracture properties, respectively. The primary effect of λvf begins at the onset of the first transitional trough (Stage IV). A higher λvf value signifies a smaller resistance to flow between the vugs and fractures, allowing for earlier and more efficient pressure support from the vug system. Consequently, as λvf increases, the first trough shifts significantly to the left (earlier times) and becomes shallower. This accelerated pressure equalization between vugs and fractures leads to an earlier start of the intermediate pseudo-radial flow (Stage V). Therefore, λvf controls the timing and shape of the transition from fracture-dominated flow to the combined fracture-vug system flow.

Figure 8 demonstrates the effect of the matrix-fracture interporosity flow coefficient, λ_{mf}, on the transient pressure response. This parameter quantifies the resistance to fluid flow from the low-permeability matrix blocks into the fracture network. The analysis shows that λ_{mf} primarily dictates the characteristics of the second interporosity flow transition, which manifests as the second trough (Stage VI) on the pressure derivative plot. Its influence is negligible on the earlier flow regimes, including the first interporosity flow regime (Stage IV), which is typically associated with vug-fracture interaction.As observed in the figure, a smaller λ_{mf} value (e.g., curve ②:10^{-11}) signifies lower resistance to flow between the matrix and fractures, enabling the matrix to supply fluid more efficiently and earlier. This results in a deeper and earlier second trough (Stage VI). Conversely, a larger λ_{mf} value (e.g., curve ①:10^{-10}) indicates higher resistance, leading to a shallower and later second trough. Therefore, λ_{mf} is crucial for quantifying the connectivity and the timing of the late-time fluid support from the matrix system.

Figure 9 presents a sensitivity analysis of the vuggy storativity ratio (ωv), with the fracture storativity ratio (ωf) held constant to isolate its effect on the pressure transient response. The results demonstrate that ωv primarily governs the dynamics of the interporosity flow regimes. A higher ωv value—representing an increased storage capacity in the vuggy system—causes the corresponding transitional trough on the pressure derivative curve to shift to an earlier time, which in turn signifies an accelerated onset of crossflow from the vuggy system into the fracture network.

Figure 10 presents a sensitivity analysis of the fracture storativity ratio (ω_f), with the vuggy storativity ratio (ω_v) held constant to isolate its effect on the pressure transient response. The results reveal that ω_f has a pronounced impact on a wide spectrum of flow regimes, including the initial skin-dominated period, the early radial flow, the intermediate transition flow, and the subsequent interporosity flow transitions. Specifically, a smaller ω_f value causes the semilog straight-line segment corresponding to the initial radial flow in the fracture system to shift to an earlier time, thereby extending the duration of this intermediate transition period. Conversely, a larger ω_f value—representing a more compressible fracture network—accelerates the onset of interporosity flow, which manifests as a deeper transitional trough on the pressure derivative curve.

5.3. Field Example Application

A pressure buildup test well was selected from the Tahe Oilfield (or the fractured-vuggy carbonate reservoirs in the Tarim Basin). This reservoir is geologically characterized by extensive paleo-karstification, creating a complex pore structure where matrix, natural fractures, and dissolution vugs (caves) coexist. This geological reality provides strong physical evidence for the triple-porosity assumption. The test was conducted from November 9th to November 20th, 2023. Based on this geological background and the diagnostic features of the pressure transient data—specifically, the presence of two distinct troughs on the pressure derivative curve—a triple-porosity, single-permeability model with transient interporosity flow was selected for curve fitting and well test interpretation. The top and bottom boundaries of the model were set to be closed, and the external boundary was treated as infinite. The oil rate for this well prior to shut-in was 86.72 m^3/d. The crucial formation and well parameters are listed in **Table 1**.

The fitted curves of well-test interpretation are shown as **Figure 11**. This figure illustrates the curves plotted from the field data and the curves run by the model exhibit a substantial level of concordance. The interpretation results are shown in **Table 2**. This example application shows the reliability and practicality of the model. It is worth noting that the interpretation yields a positive total skin factor ($S = 0.84$). Theoretically, as mentioned in the Introduction, the inclination of a slanted well typically induces a negative geometric pseudoskin effect by increasing the contact area with the formation. However, the total skin factor derived from the well test is a combination of this geometric pseudoskin and the mechanical skin caused by formation damage (e.g., mud invasion during drilling). In this specific field case, the positive value of the total skin indicates that the formation damage is significant enough to override the negative pseudoskin benefit provided by the well inclination, resulting in an overall positive skin effect. The excellent agreement between the field data and the model-generated curves, particularly the distinct troughs on

Accepted by Scientia Iranica

the derivative plot, serves as a robust validation of the proposed triple-porosity model and confirms the accuracy of the identified flow regimes.

6. Conclusions

This study presents a comprehensive semi-analytical model to characterize the pressure transient behavior of slanted wells in complex fractured-vuggy carbonate reservoirs. By conceptualizing the formation as a triple-porosity system and incorporating an unsteady-state inter-porosity flow mechanism, this work provides a more accurate representation of flow dynamics in these highly heterogeneous formations. The primary conclusions are as follows:

(1) Unique Diagnostic Signature Identified: The model reveals a unique and critical diagnostic signature for fractured-vuggy systems: two successive troughs on the pressure derivative curve. This "double-trough" feature directly corresponds to the sequential fluid feed, first from the high-conductivity vug system and subsequently from the low-permeability matrix system into the fracture network. This signature serves as a definitive tool for identifying the contributions of different porous media during well test interpretation.

(2) Quantified Impact of Well Geometry: The well inclination angle (θ) and length (L) were found to primarily influence the early- to middle-time flow regimes. An increase in either parameter leads to a systematic downward shift in both the pressure and pressure derivative curves, signifying a lower overall flow resistance. This finding is crucial for optimizing slanted well design to maximize productivity in such reservoirs.

(3) Governing Role of Inter-porosity Parameters and Critical Flow Conditions: The characteristics of the transitional flow periods are governed by the inter-porosity flow coefficients (λ_{vf} and λ_{mf}) and storativity ratios (ω_v and ω_f). Critically, the first derivative trough (vug-fracture interaction) becomes visible and deeper only when the vug system has a significant storativity ratio (ω_v) and a moderate inter-porosity flow coefficient (λ_{vf}). Similarly, the appearance of the second trough (matrix-fracture interaction) requires a substantial matrix storativity but is strictly controlled by the matrix-fracture interporosity flow coefficient (λ_{mf}); a smaller λ_{mf} ($<10^{-9}$) delays the matrix support, making the second trough distinct and separated from the first one. These critical conditions provide quantitative guidance for identifying triple-porosity behaviors.

(4) It should be noted that the current model is developed based on several simplifying assumptions, such as single-phase fluid flow, constant fluid and rock properties, and spherical shapes for both matrix blocks and vugs. While these assumptions are essential for achieving a semi-analytical solution and provide a foundational understanding of the system, they may not fully capture the complexities of real fractured-vuggy carbonate reservoirs. Future research should be directed towards incorporating more complex physics, such as multi-phase flow, stress-sensitive permeability and porosity, and non-Darcy flow effects. Extending the model to account for arbitrarily shaped matrix/vug blocks and more complex wellbore configurations would further enhance its accuracy and applicability in diverse geological settings.

Accepted by Scientia Iranica

Nomenclature

Δp_s	additional pressure drop, [MPa]
p_w	wellbore pressure [MPa]
p_i	initial pressure [MPa]
p	pressure of zone [MPa]
t	production time [h]
r	radius [m]
r_w	wellbore radius [m]
r_e	radius of side external boundary [m]
x	horizontal distance [m]
z	vertical distance from the bottom boundary [m]
z_w	vertical distance for wellbore center [m]
$\tilde{q}$	production rate of point source [m^3/d]
q	production rate at wellhead [m^3/d]
k_h	horizontal permeability of zone [μm^2]
k_p	perpendicular permeability of zone [μm^2]
C_t	total compressibility of zone [MPa^{-1}]
B	oil volume factor
L	slanted well length [m]
h	reservoir thickness [m]
C_s	wellbore storage coefficient [m^3/MPa]
C_D	dimensionless wellbore storage [coefficient]
ω_f	fracture-system storativity [ratio]
ω_m	matrix-system storativity [ratio]
ω_v	vug-system storativity [ratio]
p_{jD}	dimensionless pressure ,j=m,f,v
t_D	dimensionless time
z_D,z_{wD}	dimensionless vertical distance
r_D,r_{mD},r_{vD}	dimensionless radial distance
S_p	perpendicular well skin factor
S	total skin factor
u	Laplace transform variable
R	component of the pressure in the horizontal direction
Z	component of the pressure in the vertical direction
$\bar{}$	parameters in Laplace space
$I_0(\ )$, $K_0(\ )$	zero-order modified Bessel function of the first kind and second kind
$I_1(\ )$, $K_1(\ )$	first-order modified Bessel function of the first kind and second kind
μ	fluid viscosity of zone [mPa·s]
ϕ	porosity of zone [fraction]
θ	inclination angle [°]
ε	radius of point source [m]
ξ	intermediate substitution variable
λ_n	eigenvalue of eigenfunction
λ_{mf}	matrix-to-fracture interporosity flow coefficient
λ_{vf}	vug-to-fracture interporosity flow coefficient

Accepted by Scientia Iranica

Authors' Credit

Renshi Nie is a Professor at Southwest Petroleum University and a core member of the National Key Laboratory of Oil and Gas Reservoir Geology and Development Engineering. He holds a Ph.D. in Petroleum Engineering and focuses on reservoir engineering, well testing, and transient flow modeling.

Zipeng Xia received his B.Sc. degree in Petroleum Engineering from Southwest Petroleum University, where he is currently pursuing his M.Sc. His primary research interests include well test interpretation, analytical/semi-analytical modeling of transient flow, and characterization of naturally fractured reservoirs.

Ming Wang is a Senior Engineer with the PetroChina Tarim Oilfield Company in Korla, China. His work focuses on the development and management of complex oil and gas fields.

Jingcheng Liu is an associate researcher at the Liquor Making Microbial Application & Detection Technology of Luzhou Key Laboratory at Luzhou Vocational & Technical College. He also holds a position at the Institute of Petroleum & Gas Engineering at Chongqing University of Science and Technology. His research interests include unconventional reservoir characterization and fluid dynamics.

Tao Zhang is currently with Xi'an Sanwei Technology Development Co., Ltd. in Xi'an, China, where he is involved in the research and development of petroleum engineering software and technologies.

Cong Lu is a Professor and Ph.D. supervisor at Southwest Petroleum University. He received his B.Sc., M.Sc., and Ph.D. degrees in Petroleum Engineering from the same university. His research focuses on reservoir stimulation theory and technologies.

Fan-Hui Zeng is a Professor and Ph.D. supervisor at Southwest Petroleum University, serving as Director of the Intelligent Oil and Gas Engineering Research Center. He holds B.Sc., M.Sc., and Ph.D. degrees from Southwest Petroleum University. His research interests include enhanced oil and gas recovery, AI applications in petroleum engineering, and reservoir optimization.

Accepted by Scientia Iranica

Appendix Parameters definition

Dimensionless parameters:
Reservoir thickness

$$h_D = h\sqrt{k_h / k_p} / (r_w e^{-S}) \tag{A-1}$$

Pressure with a constant rate production

$$p_{jD} = k_h h(p_i - p_j) / (1.842\times10^{-3} qB\mu), (j = \mathrm{f}, \mathrm{m}, \mathrm{v}) \tag{A-2}$$

Radial radius

$$r_D = r / (r_w e^{-S}) \tag{A-3}$$

Production time

$$t_D = 3.6k_{fh} t / \mu r_w^{\ 2}(\phi_f C_{ft} + \phi_m C_{mt} + \phi_v C_{vt}) \tag{A-4}$$

Vertical distance

$$z_D = z / h \tag{A-5}$$

Vertical distance for wellbore center

$$z_{wD} = z_w / h \tag{A-6}$$

Wellbore storage coefficient

$$C_D = C_s / 6.2832hr_w^{\ 2}(\phi_f C_{ft} + \phi_m C_{mt} + \phi_v C_{vt}) \tag{A-7}$$

Fracture-System Elastic Storage Coefficient

$$\omega_f = \phi_f C_{ft} / (\phi_f C_{ft} + \phi_m C_{mt} + \phi_v C_{vt}) \tag{A-8}$$

Matrix-System Elastic Storage Coefficient

$$\omega_m = \phi_m C_{mt} / (\phi_f C_{ft} + \phi_m C_{mt} + \phi_v C_{vt}) \tag{A-9}$$

Vug-System Elastic Storage Coefficient

$$\omega_v = \phi_v C_{vt} / (\phi_f C_{ft} + \phi_m C_{mt} + \phi_v C_{vt}) \tag{A-10}$$

perpendicular well skin factor

$$S_p = k_h h \Delta p_s / (1.842\times10^{-3} q\mu B) \tag{A-11}$$

Total skin factor

$$S_s = \left[L / (2h\sqrt{k_{1h} / k_{1p}}) + \right] S_p \tag{A-12}$$

Spherical geometry factor

$$\alpha_j = 15 / r_{js}^2, \quad (j = \mathrm{m, v}) \tag{A-13}$$

Matrix-to-Fracture Crossflow Coefficient

$$\lambda_{mf} = \alpha_m k_m r_w^{\ 2} / k_{fh} = 15 r_w^{\ 2} k_m / r_{ms}^{\ 2} k_{fh} \tag{A-14}$$

Vug-to-Fracture Crossflow Coefficient

$$\lambda_{vf} = \alpha_v k_v r_w^{\ 2} / k_{fh} = 15 r_w^{\ 2} k_v / r_{vs}^{\ 2} k_{fh} \tag{A-15}$$

Spherical Radial Distance in the Matrix System

$$r_{mD} = r_m / r_{ms} \tag{A-16}$$

Spherical Radial Distance in the Vug System

$$r_{vD} = r_v / r_{vs} \tag{A-17}$$

Accepted by Scientia Iranica

References

1. Warren, J. E. and Root, P. J., "The behavior of naturally fractured reservoirs", *Soc. Pet. Eng. J.*, **3**(03), pp. 245–255 (1963)
https://doi.org/10.2118/426-PA.
2. Nie, R.-S., Meng, Y.-F., Jia, Y.-L., et al., "Dual porosity and dual permeability modeling of horizontal well in naturally fractured reservoir", *Transp. Porous Media*, **92**(1), pp. 213–235 (2012)
https://doi.org/10.1007/s11242-011-9898-3.
3. Li, D., Wang, J. Y., Zha, W., et al., "Pressure transient behaviors of hydraulically fractured horizontal shale-gas wells by using dual-porosity and dual-permeability model", *J. Pet. Sci. Eng.*, **164**, pp. 531–545 (2018)
https://doi.org/10.1016/j.petrol.2018.01.016.
4. Baniasadi, H. and Rashidi, F., "A triple-porosity radial composite model for two-phase well test analysis of volatile oil in fractured-vuggy reservoirs", *Sci. Iran.*, **28**(3), pp. 1378–1399 (2021)
https://doi.org/10.24200/sci.2021.55522.4262.
5. Shi, W., Cheng, J., Liu, Y., et al., "Pressure transient analysis of horizontal wells in multibranched fault-karst carbonate reservoirs: Model and application in SHB oilfield", *J. Pet. Sci. Eng.*, **220**, p. 111167 (2023)
https://doi.org/10.1016/j.petrol.2022.111167.
6. Cinco, H., Miller, F. G., and Ramey Jr., H. J., "Unsteady-State pressure distribution created by a directionally drilled well", *J. Pet. Technol.*, **27**(11), pp. 1392–1400 (1975)
https://doi.org/10.2118/5131-PA.
7. Ozkan, E. and Raghavan, R., "New solutions for well-test-analysis problems: Part 1—analytical considerations", *SPE Form. Eval.*, **6**(03), pp. 359–368 (1991)
https://doi.org/10.2118/18615-PA.
8. Guo, J.-J., Jiang, C.-Z., Wang, H.-T., et al., "Pressure transient behavior of fractured wells in multilayered tight gas reservoirs with heterogeneous properties and limited fracture height", *Pet. Sci.*, **22**(8), pp. 3357–3379 (2025)
https://doi.org/10.1016/j.petsci.2025.05.002.
9. Feng, G. and Liu, Q., "Pressure transient behavior of a slanted well with an impermeable fault", *J. Hydrodyn.*, **26**(6), pp. 980–985 (2014)
https://doi.org/10.1016/S1001-6058(14)60108-6.
10. Fair, P. S., Kikani, J., and White, C. D., "Modeling high-angle wells in laminated pay reservoirs", *SPE Reserv. Eval. Eng.*, **2**(01), pp. 46–52 (1999)
https://doi.org/10.2118/54656-PA.
11. Wang, K., Wang, L., Adenutsi, C. D., et al., "Analysis of gas flow behavior for highly deviated wells in naturally fractured-vuggy carbonate gas reservoirs", *Math. Probl. Eng.*, **2019**(1), p. 6919176 (2019)
https://doi.org/10.1155/2019/6919176.
12. Zhang, Y.-Y., Li, S.-S., and Li, L., "Pressure transient characteristics of highly deviated wells in fractured-vuggy carbonate gas reservoirs BT - proceedings of the international field exploration and development conference 2021", J. Lin, Ed., Springer Nature Singapore, Singapore, pp. 1739–1758 (2022)
https://doi.org/10.1007/978-981-19-2149-0_160.
13. Jia, P., Cheng, L., Huang, S., et al., "Pressure-Transient analysis of a finite-conductivity inclined fracture connected to a slanted wellbore", *SPE J.*, **21**(02), pp. 522–537 (2016)
https://doi.org/10.2118/178929-PA.
14. Chen, X. and Liu, P., "Pressure transient response with random distributed fracture networks using a semi-analytical method for fractured horizontal wells in a rectangular closed reservoir", *J. Hydrol.*, **607**, p. 127547 (2022)
https://doi.org/10.1016/j.jhydrol.2022.127547.
15. Hu, J., Tan, P., Zhang, C. S., et al., "A three-dimensional model of two-phase flow to a horizontal well in dual-porosity media", *Comput. Geotech.*, **185**, p. 107337 (2025)
https://doi.org/10.1016/j.compgeo.2025.107337.
16. Li, R., Zhang, C.-S., and Chen, Z., "A stokes–dual–porosity–poroelasticity model and discontinuous galerkin method for the coupled free flow and dual porosity poroelastic medium problem", *J. Sci. Comput.*, **102**(2), p. 41 (2025)
https://doi.org/10.1007/s10915-024-02771-3.
17. Moutsopoulos, K. N., Papaspyros, J. N. E., Koussis, A. D., et al., "On the flow behaviour of unconfined dual porosity aquifers with sloping base", *Adv. Water Resour.*, **195**, p. 104856 (2025)
https://doi.org/10.1016/j.advwatres.2024.104856.
18. Wang, M., Wu, K., Zhu, Q., et al., "The oil/water two-phase flow behavior of dual-porosity carbonates", Processes, 13(3), p. 713 (2025).
https://doi.org/10.3390/pr13030713.
19. Sousa, B. R. and Moreno, R. B., "Transition radial flow in slanted well test analysis", in SPE Latin American and Caribbean Petroleum Engineering Conference, p. SPE-177034-MS (2015).
https://doi.org/10.2118/177034-MS.
20. Khattab, H. A., Yeh, N.-S., and Agarwal, R. G., "Pressure transient behavior of slanted wells in single- and multiple-layered systems", SPE Form. Eval., 6(03), pp. 293–302 (1991).
https://doi.org/10.2118/22730-MS.

Accepted by Scientia Iranica

21. Dinh, A. V and Tiab, D., "Pressure-Transient analysis of a well with an inclined hydraulic fracture", *SPE Reserv. Eval. Eng.*, **13**(06), pp. 845–860 (2010)
https://doi.org/10.2118/120540-PA.
22. Liang, Y.-Z., Teng, B.-L., and Luo, W.-J., "Study of the pressure transient behavior of directional wells considering the effect of non-uniform flux distribution", *Pet. Sci.*, **21**(3), pp. 1765–1779 (2024)
https://doi.org/10.1016/j.petsci.2023.12.014.
23. Nie, R., Wang, C., Fan, X., et al., "Modeling the flow characteristics of high-velocity non-Darcy flow in gas reservoirs with heterogeneously distributed fractures", *Sci. Iran.* (2025)
https://doi.org/10.24200/sci.2025.66638.10163.
24. Ozkan, E. and Raghavan, R., "A Computationally Efficient, Transient-Pressure Solution for Inclined Wells", *SPE Reserv. Eval. Eng.*, **3**(05), pp. 414–425 (2000)
https://doi.org/10.2118/66206-PA.
25. Abbaszadeh, M. and Hegeman, P. S., "Pressure-Transient analysis for a slanted well in a reservoir with vertical pressure support", *SPE Form. Eval.*, **5**(03), pp. 277–284 (1990)
https://doi.org/10.2118/19045-PA.

Biographies

Renshi Nie is a Professor at Southwest Petroleum University and a core member of the National Key Laboratory of Oil and Gas Reservoir Geology and Development Engineering. He holds a Ph.D. in Petroleum Engineering and focuses on reservoir engineering, well testing, and transient flow modeling.

Zipeng Xia received his B.Sc. degree in Petroleum Engineering from Southwest Petroleum University, where he is currently pursuing his M.Sc. His primary research interests include well test interpretation, analytical/semi-analytical modeling of transient flow, and characterization of naturally fractured reservoirs.

Ming Wang is a Senior Engineer with the PetroChina Tarim Oilfield Company in Korla, China. His work focuses on the development and management of complex oil and gas fields.

Jingcheng Liu is an associate researcher at the Liquor Making Microbial Application & Detection Technology of Luzhou Key Laboratory at Luzhou Vocational & Technical College. He also holds a position at the Institute of Petroleum & Gas Engineering at Chongqing University of Science and Technology. His research interests include unconventional reservoir characterization and fluid dynamics.

Tao Zhang is currently with Xi'an Sanwei Technology Development Co., Ltd. in Xi'an, China, where he is involved in the research and development of petroleum engineering software and technologies.

Cong Lu is a Professor and Ph.D. supervisor at Southwest Petroleum University. He received his B.Sc., M.Sc., and Ph.D. degrees in Petroleum Engineering from the same university. His research focuses on reservoir stimulation theory and technologies.

Fan-Hui Zeng is a Professor and Ph.D. supervisor at Southwest Petroleum University, serving as Director of the Intelligent Oil and Gas Engineering Research Center. He holds B.Sc., M.Sc., and Ph.D. degrees from Southwest Petroleum University. His research interests include enhanced oil and gas recovery, AI applications in petroleum engineering, and reservoir optimization.

Accepted by Scientia Iranica

List of Figure Captions

Figure 1. Schematic Diagram of the Physical Model for a Slanted Well in a Fractured-Vuggy Carbonate Reservoir

Figure 2. Schematic of Flow Pathways in a Triple-Porosity Single-Permeability Model for a Slanted Well

Figure 3. Schematic of a Matrix Block Model

Figure 4. Flow regime identification on a typical type curve for a slanted well in a triple-porosity reservoir (Roman numerals I–VIII correspond to Stage I–VIII in the text. Other parameters are h = 30m, C_D = 500, θ = 40°, S = 2, λ_{vf} = 10−8, λ_{mf} = 10^{-10}, k_h/k_p = 3, ω_f = 0.01, ω_m = 0.94, ω_v = 0.05, z_{wD} = 0.5, and r_{eD} = 2 × 10^{-4}.).

Figure 5. Pressure transient analysis curves affected by inclination angle of slanted well.(Other parameters are h = 30 m, C_D = 500, S = 2, λ_{vf} = 10^{-8}, λ_{mf} = 10^{-10}, k_h/k_p = 3, ω_f = 0.01, ω_m = 0.94, ω_v = 0.05, z_{wD} = 0.5, and r_{wD} = 2 × 10^{-4}.)

Figure 6. Pressure transient analysis curves affected by length of slanted well.(Other parameters are h = 30 m, C_D = 500, S = 2, θ = 40°, λ_{vf} = 10^{-8}, λ_{mf} = 10^{-10}, k_h/k_p = 3, ω_f = 0.01, ω_m = 0.94, ω_v = 0.05, z_{wD} = 0.5, and r_{wD} = 2 × 10^{-4}.)

Figure 7. Pressure transient analysis curves affected by the vug-fracture interporosity flow coefficient (λ_{vf}).(Other parameters are h = 30 m, C_D = 500, S = 2, θ = 40°, λ_{mf} = 10^{-10}, k_h/k_p = 3, ω_f = 0.01, ω_m = 0.94, ω_v = 0.05, z_{wD} = 0.5, and r_{wD} = 2 × 10^{-4}.)

Figure 8. Pressure transient analysis curves affected by the matrix-fracture interporosity flow coefficient (λ_{mf}).(Other parameters are h = 30 m, C_D = 500, S = 2, θ = 40°, λ_{vf} = 10^{-8}, k_h/k_p = 3, ω_f = 0.01, ω_m = 0.94, ω_v = 0.05, z_{wD} = 0.5, and r_{wD} = 2×10^{-4}.)

Figure 9. Pressure transient analysis curves affected by the vuggy storativity ratio (ω_v).(Other parameters are h = 30 m, C_D = 500, S = 2, θ = 40°, λ_{vf} = 10^{-8}, λ_{mf} = 10^{-10}, k_h/k_p = 5, ω_f = 0.01, z_{wD} = 0.5, and r_{wD} = 2 × 10^{-4}.)

Figure 10. Pressure transient analysis curves affected by the fracture storativity ratio (ω_f).(Other parameters are h = 30 m, C_D = 500, S = 2, θ = 40°, λ_{vf} = 10^{-8}, λ_{mf} = 10^{-10}, k_h/k_p = 5, ω_v = 0.05, z_{wD} = 0.5, and r_{wD} = 2 × 10^{-4}.)

Figure 11. Fitted curves for the established model and the field data

List of Table Captions

Table 1. Formation and well parameters

Table 2. Well-test interpretation parameters

Accepted by Scientia Iranica

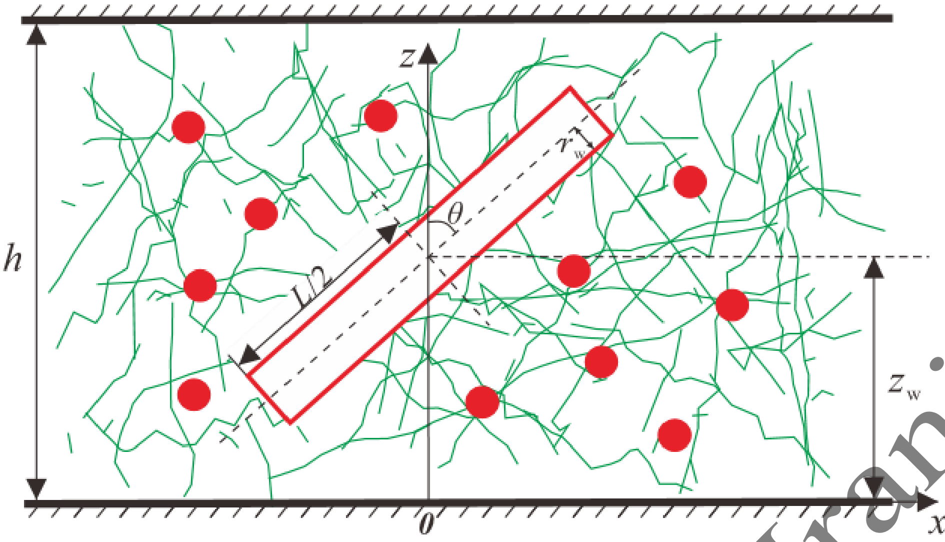

Figure 12. Schematic Diagram of the Physical Model for a Slanted Well in a Fractured-Vuggy Carbonate Reservoir

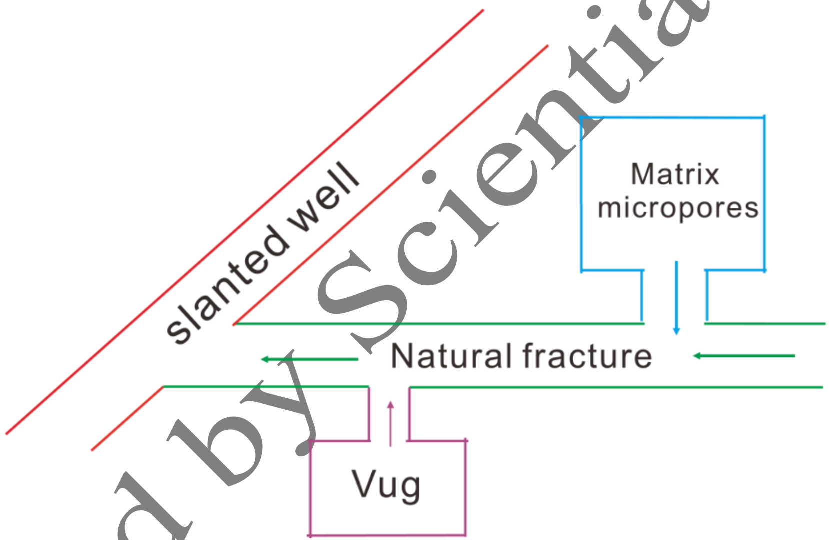

Figure 13. Schematic of Flow Pathways in a Triple-Porosity Single-Permeability Model for a Slanted Well

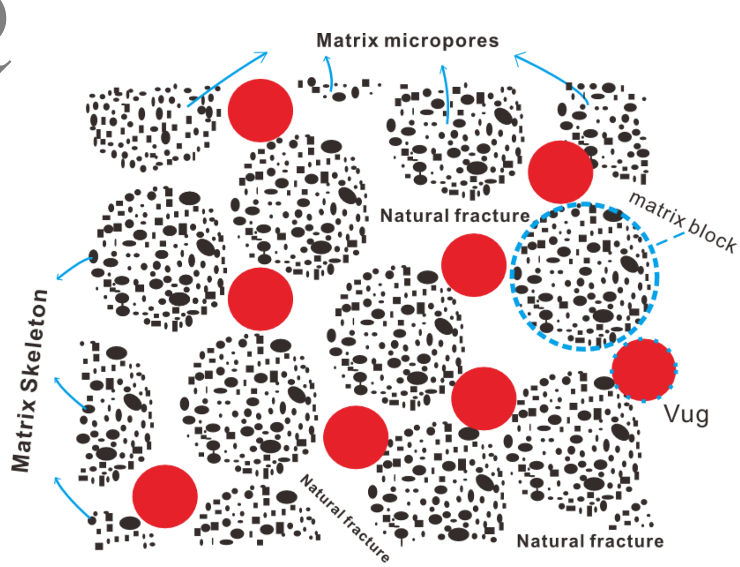

Figure 14. Schematic of a Matrix Block Model

Accepted by Scientia Iranica

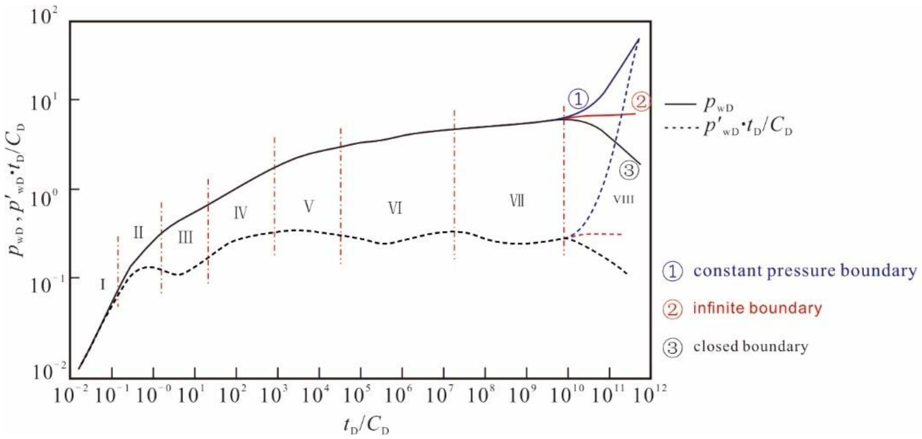

Figure 15. Flow regime identification on a typical type curve for a slanted well in a triple-porosity reservoir (Roman numerals I–VIII correspond to Stage I–VIII in the text. Other parameters are h = 30m, C_D = 500, $\theta = 40°$, $S = 2$, $\lambda_{vf} = 10-8$, $\lambda_{mf} = 10^{-10}$, $k_h/k_p = 3$, $\omega_f = 0.01$, $\omega_m = 0.94$, $\omega_v = 0.05$, $z_{wD} = 0.5$, and $r_{eD} = 2 \times 10^{-4}$.).

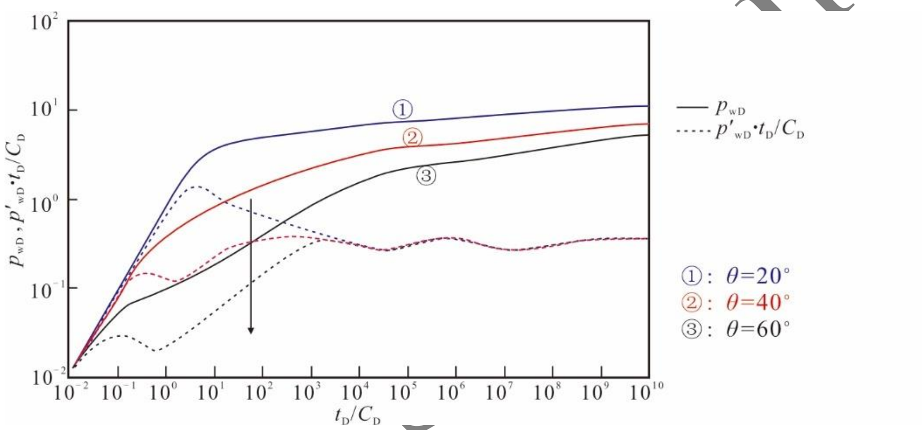

Figure 16. Pressure transient analysis curves affected by inclination angle of slanted well.(Other parameters are h = 30 m, C_D = 500, $S = 2$, $\lambda_{vf} = 10^{-8}$, $\lambda_{mf} = 10^{-10}$, $k_h/k_p = 3$, $\omega_f = 0.01$, $\omega_m = 0.94$, $\omega_v = 0.05$, $z_{wD} = 0.5$, and $r_{wD} = 2 \times 10^{-4}$.)

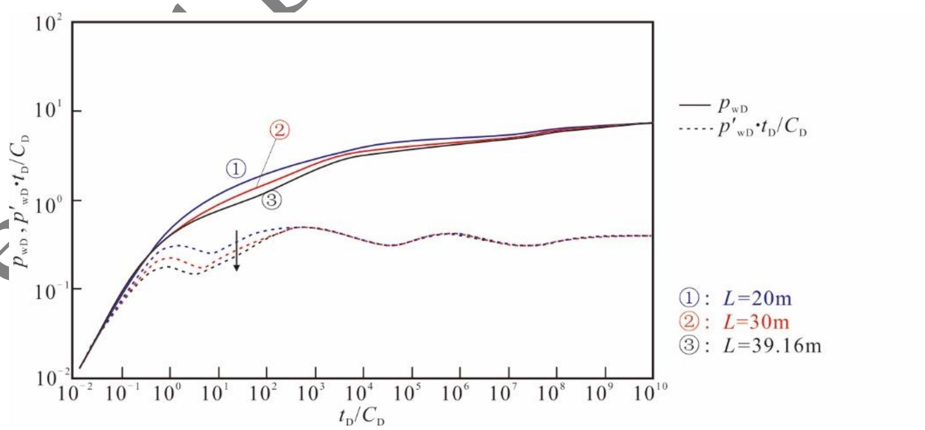

Figure 17. Pressure transient analysis curves affected by length of slanted well.(Other parameters are h = 30 m, C_D = 500, $S = 2$, $\theta = 40°$, $\lambda_{vf} = 10^{-8}$, $\lambda_{mf} = 10^{-10}$, $k_h/k_p = 3$, $\omega_f = 0.01$, $\omega_m = 0.94$, $\omega_v = 0.05$, $z_{wD} = 0.5$, and $r_{wD} = 2 \times 10^{-4}$.)

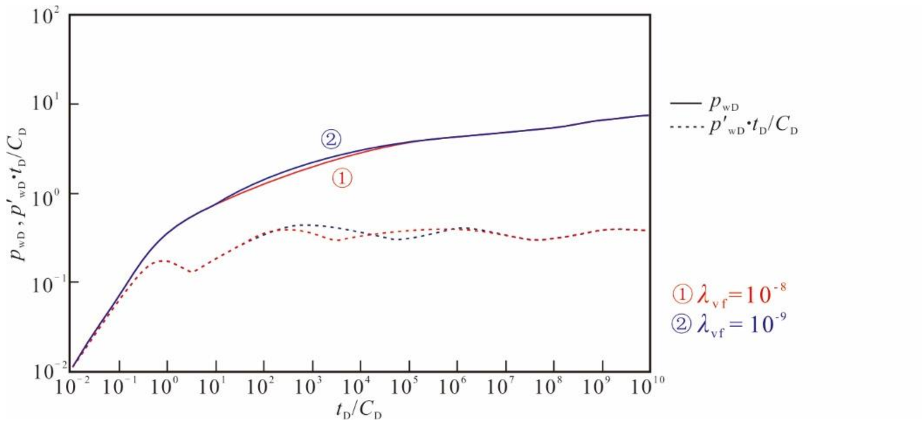

Figure 18. Pressure transient analysis curves affected by the vug-fracture interporosity flow coefficient (λ_{vf}).(Other parameters are h = 30 m, C_D = 500, S = 2, θ = 40°, $\lambda_{mf} = 10^{-10}$, k_h/k_p = 3, ω_f = 0.01, ω_m = 0.94, ω_v = 0.05, z_{wD} = 0.5, and $r_{wD} = 2 \times 10^{-4}$.)

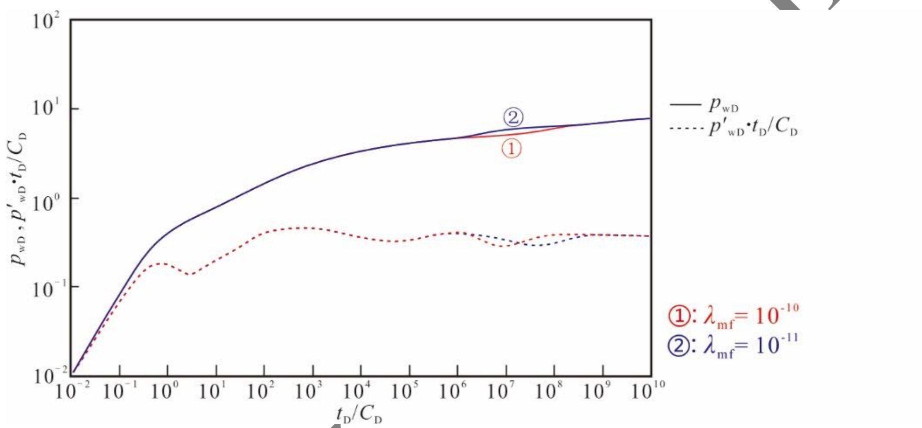

Figure 19. Pressure transient analysis curves affected by the matrix-fracture interporosity flow coefficient (λ_{mf}).(Other parameters are h = 30 m, C_D = 500, S = 2, θ = 40°, $\lambda_{vf} = 10^{-8}$, k_h/k_p = 3, ω_f = 0.01, ω_m = 0.94, ω_v = 0.05, z_{wD} = 0.5, and $r_{wD} = 2\times10^{-4}$.)

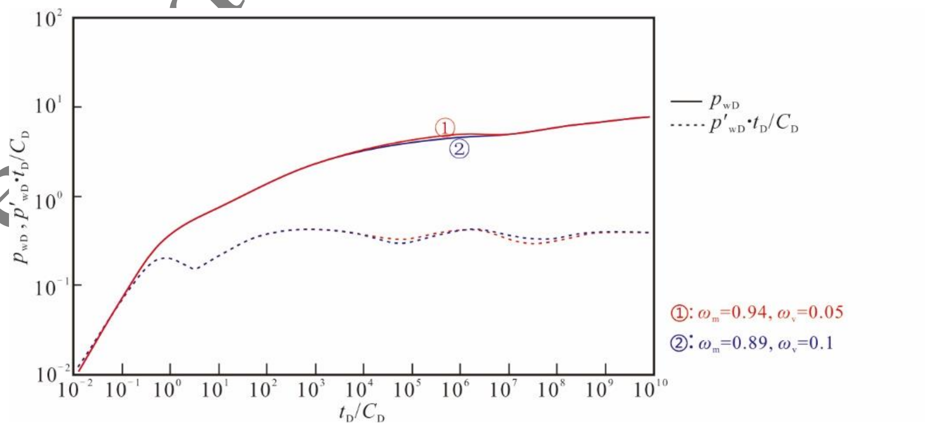

Figure 20. Pressure transient analysis curves affected by the vuggy storativity ratio (ω_v).(Other parameters are h = 30 m, C_D = 500, S = 2, θ = 40°, $\lambda_{vf} = 10^{-8}$, $\lambda_{mf} = 10^{-10}$, k_h/k_p = 5, ω_f = 0.01, z_{wD} = 0.5, and $r_{wD} = 2 \times 10^{-4}$.)

Accepted by Iranica

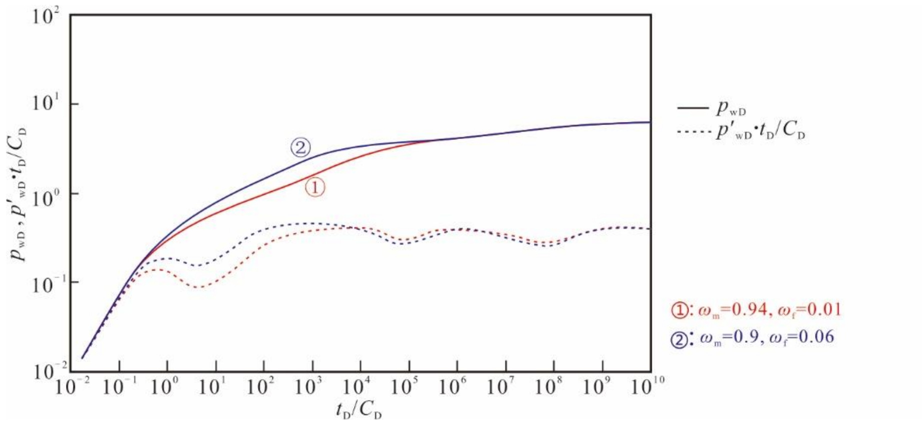

Figure 21. Pressure transient analysis curves affected by the fracture storativity ratio (ω_f).(Other parameters are h = 30 m, C_D = 500, S = 2, θ = 40°, λ_{vf} = 10^{-8}, λ_{mf} = 10^{-10}, k_h/k_p = 5, ω_v = 0.05, z_{wD} = 0.5, and r_{wD} = 2 × 10^{-4}.)

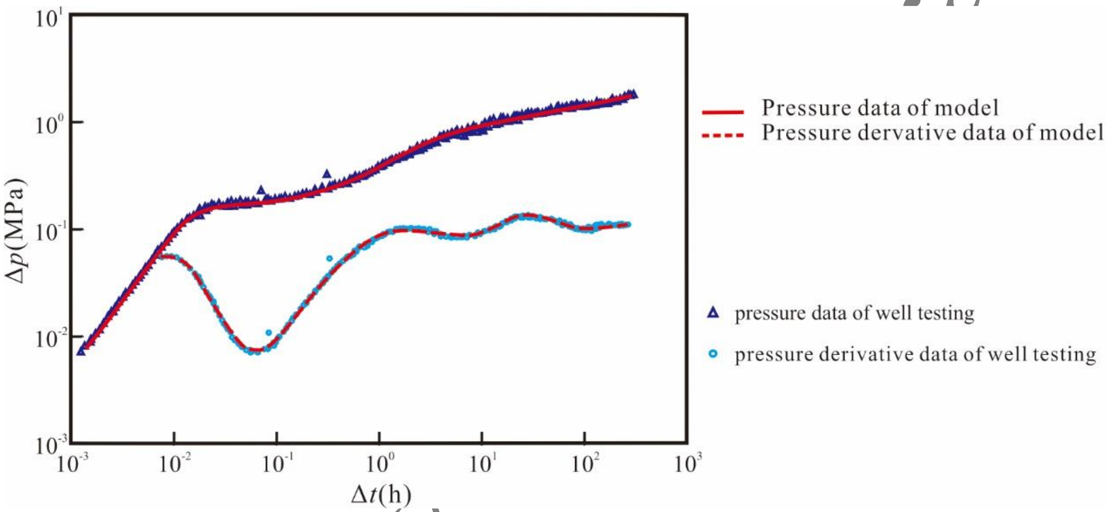

Figure 22. Fitted curves for the established model and the field data

h (m)	μ (mPa·s)	ϕ_m	ϕ_f	ϕ_v	B	C_t (10^{-3}MPa^{-1})	r_w (m)	L (m)	θ (°)
173.07	0.684	0.048	0.0013	0.12	1.28	1.19	0.07	89.14	60

Table 3. Formation and well parameters

k_h (10^{-3}μm^2)	K_p (10^{-3}μm^2)	k_h/k_p	ω_f	ω_v	S	λ_{vf}	λ_{mf}	C_s (m^3/MPa)
73.03	6.98	10.46	0.05	0.13	0.84	6.43×10^{-7}	3.17×10^{-9}	0.043

Table 4. Well-test interpretation parameters

Accepted by